Cracking of Hydrocarbons on Zeolite Catalysts: Density Functional and Hartree−Fock Calculations on the Mechanism of the β-Scission Reaction

M. V. Frash,*,† V. B. Kazansky,† A. M. Rigby,‡ and R. A. van Santen§

Zelinsky Institute of Organic Chemistry, Russian Academy of Sciences, Moscow B-334, Russia; Shell Research and Technology Centre Amsterdam, P.O. Box 3800, 1030 BN Amsterdam, The Netherlands; and Eindhoven University of Technology, P.O. Box 513, Eindhoven, The Netherlands

Received: October 1, 1997; In Final Form: January 9, 1998

Quantum chemical calculations on the mechanism of the β-scission reaction in zeolites were performed using density functional theory and Hartree−Fock methods. The results obtained indicate that the potential energy surface for this reaction is very complex. Three reaction paths were identified: path RL, one-step via the "ringlike" transition state (TS); path HBCP, via the "hydrogen-bonded" TS and substituted cyclopropane; and path HB, one-step via the "hydrogen-bonded" TS. Transition states in all reaction paths represent complexes of the carbocation-like fragment with the negatively charged cluster, whereas both initial and final states represent alkoxy species with a covalent bond between a carbon atom of the hydrocarbon portion and a zeolite oxygen. The dependence of calculated activation energy on the cluster model of zeolite and on the calculation level is discussed. The B3LYP/6-31++G**//B3LYP/6-31G* activation energies for β-scission of but-1-oxy and pent-2-oxy with the $H_3Si(OH)AlH_2(OSiH_3)$ cluster were found to be 57.4 and 52.4 kcal/mol, respectively.

1. Introduction

Catalytic cracking of paraffins in zeolites is one of the most important processes in the modern refinery.[1,2] Extensive experimental studies of catalytic cracking have been performed, and their results indicated that cracking might follow either the protolytic or the chain mechanism.[3−14] The former consists of a direct cleavage of a carbon−carbon bond of alkane by the zeolite proton:

$$\mathrm{R1{-}|{-}CH_2{-}CH_2{-}R2 + H{-}OZ \Rightarrow R1{-}H + R2{-}CH_2{-}CH_2{-}OZ \Rightarrow R1{-}H + R2{-}CH{=}CH_2 + H{-}OZ} \quad (1)$$

whereas the latter mechanism includes hydride transfer and β-scission steps:

$$\mathrm{R1{-}CH_2{-}CH_2{-}R2 + R3{-}OZ \Rightarrow R3{-}H + R1{-}CH_2{-}CH(R2){-}OZ} \quad (2a)$$

$$\mathrm{R1{-}|{-}CH_2{-}CH(R2){-}OZ \Rightarrow R1{-}OZ + CH_2{=}CH{-}R2} \quad (2b)$$

Protolytic cracking of paraffins (eq 1) is found to be predominant under special conditions (i.e., high temperatures, low conversions, and absence of unsaturated impurities in the feed) only. This reaction is frequently used in mechanistic studies since its product composition is relatively simple and the activation energy can be directly measured. Lercher et al.[14] have shown that the true activation energy for protolytic cracking of linear alkanes from propane to *n*-hexane on H−ZSM-5 is almost independent of the number of carbon atoms.

In industrial cracking the chain process (eq 2) is predominant, due to high conversions and presence of unsaturated impurities in the feed. The measurement of the activation energies of elementary reaction steps in this case is quite difficult since a number of parallel reactions occur simultaneously. However, a comparison of activation energies for different hydrocarbons can be made based on the final product distribution.

The product distribution can be rationalized on the basis of carbenium ion theory.[15] The more stable both the carbenium ions (initial and final) involved in the β-scission reaction are, the easier it occurs.[3−7] Hydrocarbons with a larger number of carbon atoms undergo β-scission faster, since their cleavage proceeds via more stable tertiary and/or secondary carbenium ions. This holds even for linear hydrocarbons as their β-scission is often preceded by skeletal isomerization to branched products.[4,5,7] Diffusion effects and restricted transition-state shape selectivity also influence the cracking product distribution.[4]

Besides experimental techniques, quantum chemical calculations are nowadays being used in studies of the reactions catalyzed by solid acids for more detailed understanding of their molecular mechanisms.[16−18] Thus, the results of calculations indicated that the relatively stable intermediates of hydrocarbon transformations in zeolites are not carbocations but alkoxy groups covalently bound to the zeolite lattice. The carbocations represent high-energy activated complexes or transition states.[19−25] Detailed calculations on the H−D exchange between the acid site and methane showed that the approach could quantitatively describe the differences in reactivity between zeolites.[23,25]

A number of recent quantum chemical studies dealt with protolytic cracking[24,26−30] and hydride transfer[24,30] reactions. In contrast, to our best knowledge the β-scission reaction in zeolites was considered so far in one quantum chemical paper[24] only. That study reported calculations on a wide range of commercially important hydrocarbon reactions. The calculations however were performed at a modest level (MP2/6-31G*//HF/3-21G) and with symmetry constraints imposed on the geom-

† Russian Academy of Sciences.
‡ Shell Research and Technology Centre Amsterdam.
§ Eindhoven University of Technology.

S1089-5647(97)03203-3 CCC: $15.00
Published on Web 02/28/1998

TABLE 1: Total Energies (in AU) and Zero-Point Energies (ZPE, in kcal/mol) of the Initial Alkoxy Groups and the Corresponding Transition States for β-Scission[a]

		alkoxy			TS		
level, cluster		total energy	ZPE	path	total energy	IF	ZPE
B3LYP, Z_1	C_4	−553.188 854 9	105.2	RL	−553.069 531 5	−426	100.8
B3LYP, Z_1	C_4	−553.188 854 9	105.2	HBCP	−553.072 171 4	−339	100.8
B3LYP, Z_2	C_4	−1134.657 221 0	125.6	HBCP	−1134.554 472 8	−264	121.2
B3LYP/D95(d), Z_2	C_4	−1134.710 391 8	125.0	HBCP	−1134.606 342 2	−268	120.7
B3LYP, Z_1	C_5	−592.508 415 5	122.6	HBCP	−592.399 877 5	−335	118.7
B3LYP, Z_2	C_5	−1173.973 574 6	143.1	HBCP	−1173.880 125 5	−311	139.0
HF, Z_1	C_5	−589.763 519 2	130.7	HB	−589.642 769 1	−301	126.5
HF, Z_2	C_5	−1170.005 456 6	152.8	HB	−1169.902 503 2	−253	148.3

[a] Imaginary frequencies (IF, in cm^{-1}) of the transition states. B3LYP and HF mean geometry optimization at the B3LYP/6-31G* and HF/6-31G* levels, respectively. Z_1 = H(OH)AlH_2(OH); Z_2 = H_3Si(OH)AlH_2($OSiH_3$); C_4 = but-1-oxy; C_5 = pent-2-oxy.

etries of the species involved. Thus, the issues considered in that study deserve further and more detailed investigation.

In the present paper we report calculations on the mechanism of the β-scission reaction performed using the density functional (DFT) and Hartree−Fock methods and without symmetry constraints. β-Scission of but-1-oxy and pent-2-oxy will be compared, and the effects of model cluster size and of calculation level will be tested.

2. Models and Computational Details

All the calculations were performed with the Gaussian 94 program.[31] The natural population analysis (NPA) based charges[32] were computed using the natural bond orbital (NBO) package[33] of the Gaussian 94 program.

The catalytically active Brønsted acid sites of zeolites were modeled using the cluster approach which has proven to be quite useful in studies of the mechanisms of zeolite-catalyzed reactions (see refs 17−24 in the paper of Viruela-Martin et al.,[22] reviews,[16−18] and recent works[34−49]). Clusters H(OH)AlH_2(OH) and H_3Si(OH)AlH_2($OSiH_3$) were used, and the results obtained with these two clusters were compared.

The geometries of the species involved were fully optimized using the nonlocal density functional B3LYP method (the Becke three-parameter hybrid exchange[50] with the Lee−Parr−Yang correlation[51] functional) with the split-valence Pople 6-31G* basis set[52] and in the case of but-1-oxy β-scission on the H_3-Si(OH)AlH_2($OSiH_3$) cluster also with the full double-ζ Dunning D95(d) basis set.[53] For comparison, geometry optimization at the Hartree−Fock level (HF/6-31G*) was also performed. The calculated total energies, zero-point energies, and imaginary frequencies of the relevant structures are given in Table 1. To test the sensitivity of the activation energies to the level of the final energy calculations, the B3LYP, HF, and MP2 single-point energies with the 6-31G* and 6-31++G**[52] basis sets were computed for the B3LYP/6-31G* and HF/6-31G* optimized geometries.

Transition-state (TS) structures were characterized by analyzing the (analytically calculated harmonic) vibrational normal modes and by a local minimum search (after a small distortion of a TS in the reaction coordinate direction) to reach reagents and products. The computed relative energies of all species involved were corrected for the zero-point energies (ZPE) obtained from the vibrational modes calculations (unscaled frequencies were used).

3. Results

The previously reported[24] calculations on the β-scission mechanism were performed at a modest theory level (optimization HF/3-21G, single-point MP2/6-31G*) and with symmetry constraints. Now β-scission of but-1-oxy and pent-2-oxy

$$CH_3-CH_2-|-CH_2-CH_2-|-OZ \Rightarrow CH_3-CH_2-OZ + CH_2=CH_2 \quad (3)$$

$$CH_3-CH_2-|-CH_2-(CH_3-)CH-|-OZ \Rightarrow CH_3-CH_2-OZ + CH_2=CH-CH_3 \quad (4)$$

will be considered without symmetry constraints. Different cluster models of zeolite (Z_1 = H(OH)AlH2(OH), Z_2 = H_3Si-(OH)AlH2($OSiH_3$)), levels of the geometry optimization (B3LYP/6-31G*, B3LYP/D95(d), and HF/6-31G*), and the final energy calculation (B3LYP, HF, and MP2 with the 6-31G* and 6-31++G** basis sets) will be compared.

Lifting of the symmetry constraints resulted in a significant complication of the potential energy surface. Two reaction paths were found with the B3LYP/6-31G* geometry optimization procedure: the first is the one-step path via the "ringlike" TS, and the second is the two-step path via the substituted cyclopropane and the "hydrogen-bonded" TS. In contrast, the HF/6-31G* geometry optimization predicts the third reaction path—the one-step path via the "hydrogen-bonded" TS.

3.1. Path via the "Ringlike" Transition State Found at the B3LYP/6-31G* Level (Path RL). The "ringlike" TS for the β-scission reaction found earlier[24] with symmetry constraints was used in our unconstrained calculations as a starting point. However, it has been found that only a combination of the C_4 alkoxy, Z_1 cluster, and B3LYP/6-31G* geometry optimization leads to the "ringlike" TS shown in Figure 1. When any other combination is considered, a hydrogen bond between the H(1) hydrogen and the O(1) oxygen (see Figures 2, 3, and 5) is formed, resulting in other types of TS described in the next sections.

Geometry parameters of the "ringlike" TS indicate a simultaneous rearrangement of several bonds (see Table 2). Indeed, the O(1)−C(1) (2.578 Å) and C(2)−C(3) (2.083 Å) bonds cleave in the reaction while the O(2)−C(3) bond (2.341 Å) forms. The C(1)−C(2) bond (1.370 Å) changes from a single to a double bond.

The calculated activation energy for β-scission of but-1-oxy via the "ringlike" TS is 70.5 kcal/mol at the B3LYP/6-31G* and 66.5 kcal/mol at the B3LYP/6-31++G**//B3LYP/6-31G* level (see Table 3). It is interesting that the "hydrogen-bonded" TS for the same reaction on the same Z_1 cluster can be found (see the next section) and is slightly lower in energy (by 1.7 kcal/mol at the former and by 2.5 kcal/mol at the latter level). Thus, the path RL via the "ringlike" TS is calculated to be slightly less favorable than the path via the "hydrogen-bonded" TS.

3.2. Path via the "Hydrogen-Bonded" Transition State and Substituted Cyclopropane Found at the B3LYP/6-31G* Level (Path HBCP). The "hydrogen-bonded" TS was located in the B3LYP/6-31G* geometry optimization for both C_4 and C_5 alkoxy and both Z_1 and Z_2 clusters (see Figures 2 and 3). Geometry parameters of this TS given in Table 2 indicate that the TS can be considered as a complex of olefin (ethene or propene), ethyl group, and the zeolite cluster. For the (C_4 + Z_2), (C_5 + Z_1), and (C_5 + Z_2) combinations only this TS can be found even when the "ringlike" starting geometry is used.

For the (C_4 + Z_1) combination both the "hydrogen-bonded" and "ringlike" TS can be located dependent on the starting geometry (see the previous section). Formation of the O(1)−H(1) hydrogen bond in the TS of Figure 2 causes changes in other geometry parameters with respect to the "ringlike" TS of Figure 1. In particular, the C(1) atom in the former TS is at a larger distance from the O(1) oxygen (3.148 vs 2.578 Å) and much closer to the C(3) carbon (2.186 vs 2.638 Å) than in the latter TS.

The forward direction of the reaction coordinate leads from the "hydrogen-bonded" TS to the final surface alkoxy plus olefin. On the other hand, the reverse direction leads not to the initial alkoxy, but to the substituted cyclopropane plus the free Brønsted acid site. Thus, an additional reaction step—formation of the substituted cyclopropane from the initial alkoxy (5a, 6a)—should be included in the reaction path HBCP. Such a reaction path is somewhat surprising since rupture of one C(2)−C(3) bond requires initial *formation* of the new C(1)−C(3) bond followed by the simultaneous rupture of two C−C bonds:

$$CH_3{-}CH_2{-}CH_2{-}CH_2{-}OZ \Rightarrow CH_3{-}c\text{-}C_3H_5 + HOZ \quad (5a)$$

$$CH_3{-}c\text{-}C_3H_5 + HOZ \Rightarrow CH_3{-}CH_2{-}OZ + CH_2{=}CH_2 \quad (5b)$$

$$CH_3{-}CH_2{-}CH_2{-}(CH_3{-})CH{-}OZ \Rightarrow (CH_3)_2{-}c\text{-}C_3H_4 + HOZ \quad (6a)$$

$$(CH_3)_2{-}c\text{-}C_3H_4 + HOZ \Rightarrow CH_3{-}CH_2{-}OZ + CH_2{=}CH{-}CH_3 \quad (6b)$$

The transition states for methylcyclopropane formation from but-1-oxy on both the Z_1 and Z_2 clusters were located (Figure 4) and appear to be 8.0 and 5.0 kcal/mol, respectively, lower in energy (at the B3LYP/6-31++G**//B3LYP/6-31G* level with ZPE corrections) than the corresponding "hydrogen-bonded" TS for β-scission. Given such a large difference, one can suggest that for pent-2-oxy the "hydrogen-bonded" TS will also be the highest point on the reaction path. Thus, the overall activation energy for β-scission is the difference in total energies of the initial alkoxy and the "hydrogen-bonded" TS.

Table 3 shows the calculated activation energies for the β-scission reaction of but-1-oxy and pent-2-oxy on the Z_1 and Z_2 clusters. The data in this table indicate that β-scission of pent-2-oxy is around 5 kcal/mol easier than that of but-1-oxy. Thus, an additional methyl group at the reaction center stabilizes the transition state with respect to the initial state. This is in line with the experimental data since it is known[3−7] that β-scission occurs easier in larger hydrocarbons which yield alkoxy groups with more branches.

Further, one notes that the activation energies found with the larger Z_2 cluster are around 8 kcal/mol lower than those found with the smaller Z_1 cluster (for the same alkoxy). This is most likely connected with the higher acid strength of the Z_2 cluster with respect to the Z_1 cluster (deprotonation energies at the B3LYP/6-31++G**//B3LYP/6-31G* level are 319.2 and 301.9 kcal/mol, respectively). Indeed, the negative charge located on the cluster portion of the TS (e.g., −0.686 *e* on the Z_2 cluster in the TS for pent-2-oxy β-scission) can be easier distributed over the larger Z_2 cluster, and this is important for stabilization of the TS. Since the acid strength of the Z_2 cluster is still lower than that of an "average" zeolite (deprotonation energy 295 kcal/mol[54]), one can expect that the calculated β-scission activation energy will decrease if the cluster size increases. The dependence of the activation energy on the level of calculations will be considered in section 3.4.

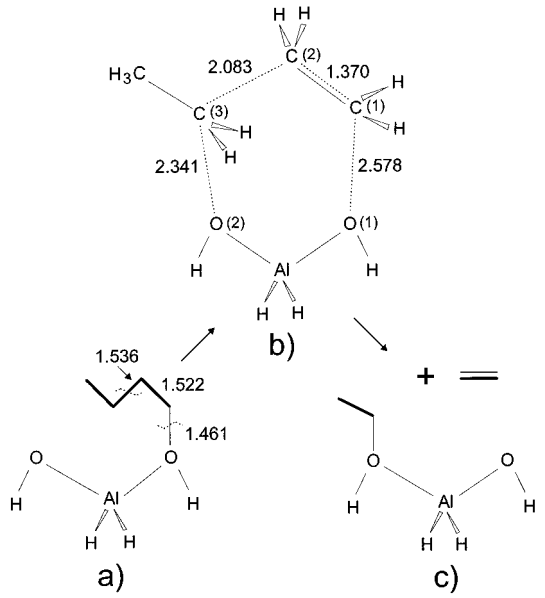

Figure 1. One-step β-scission of but-1-oxy via the "ringlike" transition state: (a) but-1-oxy; (b) TS; (c) ethoxy + ethene. Cluster $H(OH)AlH_2$-OH, B3LYP/6-31G* geometry optimization. Distances are in angstroms.

3.3. Path via the "Hydrogen-Bonded" TS Found at the HF/6-31G* Level (Path HB). For comparison purposes a search for the β-scission TS at the HF/6-31G* level was also performed. Only the "hydrogen-bonded" TS for the pent-2-oxy β-scission with both the Z_1 and Z_2 clusters has been located at this level. A similar stationary point with one imaginary frequency was also found for the but-1-oxy β-scission. However, it was not possible to find the corresponding reaction path from this stationary point to the initial but-1-oxy species. Therefore, the HF/6-31G* paths for the but-1-oxy β-scission will not be considered. No "ringlike" transition states for any alkoxy were found at the HF/6-31G* level.

Although the HF/6-31G* "hydrogen-bonded" TS shown in Figure 5 looks quite similar to the B3LYP/6-31G* "hydrogen-bonded" TS of Figure 3, the corresponding HF/6-31G* reaction path HB is different from the B3LYP/6-31G* path HBCP described in the previous section. Indeed, the former path leads from the TS directly to the pent-2-oxy species, and the substituted cyclopropane is not involved.

Thus, the HF/6-31G* description of the β-scission reaction seems to be in a better agreement with "chemical intuition" than the B3LYP/6-31G* description, since the former includes a direct one-step process whereas the latter involves two steps with formation of a new C−C bond followed by simultaneous rupture of two C−C bonds. This is somewhat surprising because it is known that usually the B3LYP functional provides a more reliable description of the reaction mechanisms than the

TABLE 2: Geometry Parameters (in angstroms) of the Transition States for β-Scission[a]

	but-1-oxy				pent-2-oxy			
distance	RL, Z_1 B3LYP	HBCP, Z_1 B3LYP	HBCP, Z_2 B3LYP	HBCP, Z_2 B3LYP/D95(d)	HBCP, Z_1 B3LYP	HBCP, Z_2 B3LYP	HB, Z_1 HF	HB, Z_2 HF
O2−C3	2.341	2.455	2.382	2.397	2.427	2.302	2.452	2.427
O1−H1	2.120	1.787	2.090	2.132	1.945	2.103	1.925	2.120
O1−C1	2.578	3.148	3.359	3.326	3.406	3.354	3.335	3.506
C1−C2	1.370	1.359	1.353	1.360	1.368	1.358	1.346	1.339
C1−C3	2.638	2.186	2.344	2.341	2.375	2.621	2.385	2.600
C2−C3	2.083	2.089	2.311	2.311	2.094	2.302	2.203	2.388

[a] RL, HBCP, and HB, reaction paths. B3LYP and HF mean geometry optimization at the B3LYP/6-31G* and HF/6-31G* levels, respectively. Z_1 = H(OH)AlH_2(OH); Z_2 = H_3Si(OH)AlH_2($OSiH_3$).

TABLE 3: Activation Energies (in kcal/mol, Including the ZPE Corrections) for β-Scission of But-1-oxy and Pent-2-oxy via Paths RL and HBCP (B3LYP/6-31G* Geometry Optimization)[a]

	but-1-oxy, RL	but-1-oxy, HBCP		pent-2-oxy, HBCP	
final energy calculation	cluster Z_1	cluster Z_1	cluster Z_2[b]	cluster Z_1	cluster Z_2
B3LYP/6-31G*	70.5	68.8	60.1	64.3	54.5
B3LYP/6-31++G**	66.5	64.0	57.4	59.6	52.4
ZPE contribution	−4.4	−4.4	−4.4	−3.9	−4.1

[a] Z_1 = H(OH)AlH_2(OH); Z_2 = H_3Si(OH)AlH_2($OSiH_3$). [b] The B3LYP/D95(d) and B3LYP/D95++(d,p)//B3LYP/D95(d) activation energies are 61.0 and 58.9 kcal/mol, respectively. The B3LYP/D95(d) ZPE contribution is −4.3 kcal/mol.

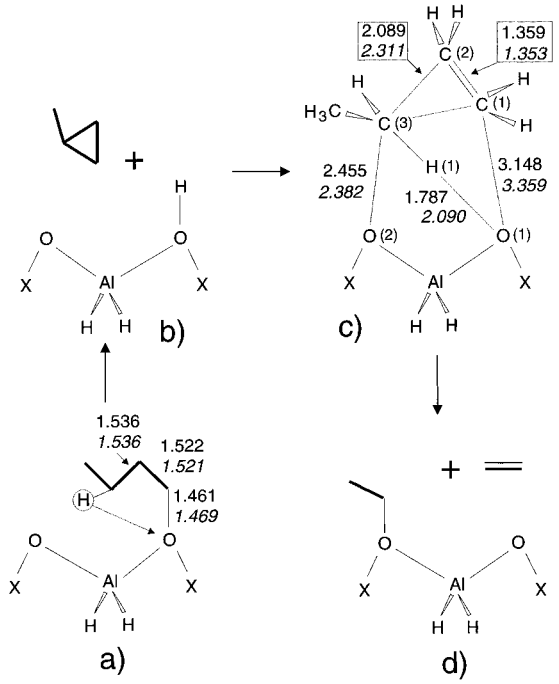

Figure 2. Two-step β-scission of but-1-oxy via the "hydrogen-bonded" transition state and methylcyclopropane: (a) but-1-oxy; (b) methylcyclopropane + cluster; (c) TS; (d) ethoxy + ethene. B3LYP/6-31G* geometry optimization. Distances are in angstroms. Straight figures, X = H; italic figures, X = SiH_3.

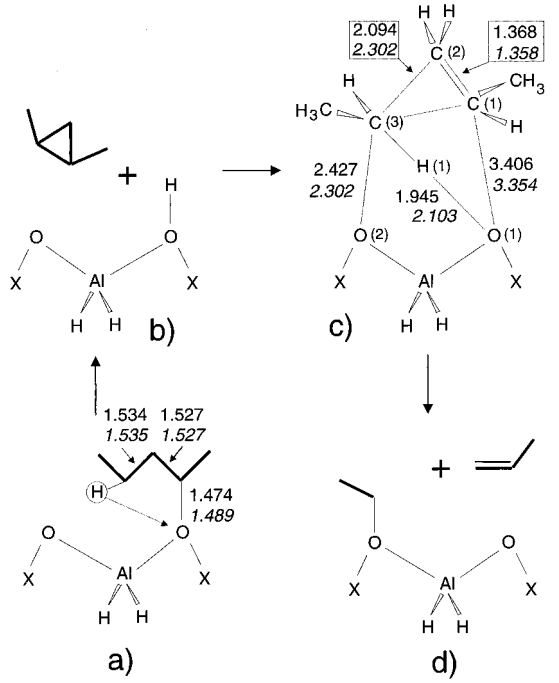

Figure 3. Two-step β-scission of pent-2-oxy via the "hydrogen-bonded" transition state and 1,2-dimethylcyclopropane: (a) pent-2-oxy; (b) 1,2-dimethylcyclopropane + cluster; (c) TS; (d) ethoxy + propene. B3LYP/6-31G* geometry optimization. Distances are in angstroms. Straight figures, X = H; italic figures, X = SiH_3.

HF functional. A possible cause of this may be the shortcoming of the cluster approach used to simulate the zeolite. The electrostatic field of a real zeolite cage which stabilizes a carbocation like TS[55] is not taken into account in the cluster calculations, and this might enforce a trend to transfer the H(1) hydrogen of the TS (Figures 2, 3, and 5) to the O(1) oxygen. On the other hand, the HF methods are known to underestimate the strength of the hydrogen-bonding interaction. Thus, the two errors might partially cancel each other, leading to more "intuitive" results in the HF than in the B3LYP calculations.

3.4. Dependence of Activation Energy on the Level of Calculations. Sensitivity of the activation energy to the improvement of basis set used for geometry optimization was tested by comparing the B3LYP/6-31G* and B3LYP/D95(d) results for but-1-oxy β-scission on the Z_2 cluster. Data of Table 3 indicate that the difference between the B3LYP/6-31G* and B3LYP/D95(d) values is 0.9 kcal/mol only. The B3LYP/D95++(d,p)//B3LYP/D95(d) activation energy differs from the B3LYP/6-31++G**//B3LYP/6-31G* value by 1.5 kcal/mol only. The B3LYP/6-31G* and B3LYP/D95(d) optimized geometries appear to be quite similar, the difference in bond lengths being no larger than 0.012 Å for the initial state and 0.042 Å for the transition state. Thus, it was concluded that the 6-31G* basis set is sufficient for geometry optimization of the species under consideration, and basis set improvement is not crucial.

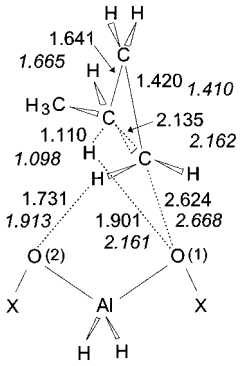

Figure 4. Transition state for formation of methylcyclopropane from but-1-oxy. B3LYP/6-31G* geometry optimization. Distances in angstroms. Straight figures, X = H; italic figures, X = SiH_3.

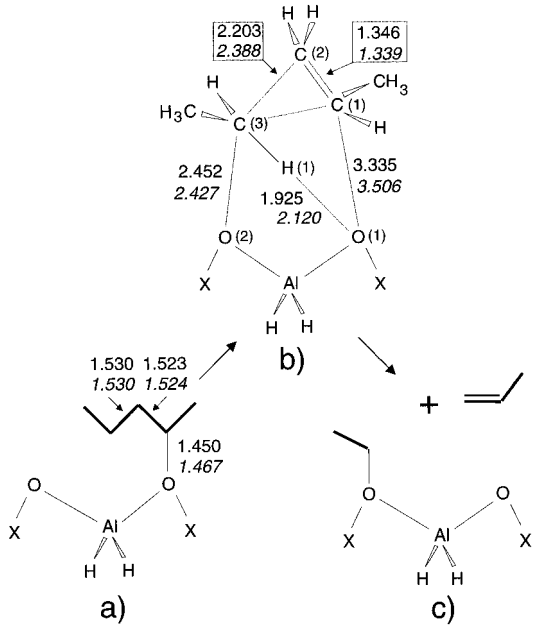

Figure 5. One-step β-scission of but-1-oxy via the "hydrogen-bonded" transition state: (a) pent-2-oxy; (b) TS; (c) ethoxy + propene. HF/6-31G* geometry optimization. Distances are in angstroms. Straight figures, X = H; italic figures, X = CH_3.

Further comparisons will be made using an example of pent-2-oxy β-scission, since both the B3LYP/6-31G* and HF/6-31G* paths are available for this reaction. Table 4 contains the HF, MP2, and B3LYP activation energies found with the B3LYP/6-31G* and HF/6-31G* geometries. The data of Table 4 show that the B3LYP activation energies are lower by around 7 kcal/mol than the HF ones, which are in turn lower by around 2 kcal/mol than the MP2 values. Further, it is interesting that geometry optimizations at the B3LYP/6-31G* and HF/6-31G* levels, albeit predicting different reaction paths, lead to close (within 2.1 kcal/mol) values for $E^{\#}$ provided that final energy calculations are performed at the same level. This is likely to be caused by the similarity of the TS geometries found at both the B3LYP/6-31G* and HF/6-31G* levels. Finally, the activation energies found with the 6-31++G** basis set are lower by around 4 kcal/mol than those with the 6-31G* basis set. A possible cause for this might be the better description of the negatively charged oxygen atoms of the TS with the 6-31++G** basis set due to the diffuse functions incorporated in this set.

4. Discussion

The above presented results indicate that the potential energy surface for the β-scission reaction is very complex. Three possible reaction paths were found: path RL, one-step via the "ringlike" TS; path HBCP, two-step via the "hydrogen-bonded" TS and substituted cyclopropane; and path HB, one-step via the "hydrogen-bonded" TS. The calculated lowest energy path HBCP is a rather surprising one since it requires initial formation of the new C−C bond followed by the simultaneous cleavage of two C−C bonds. As was pointed out in section 3.3, this might be an artifact of the cluster approach.

It is interesting to note that participation of the substituted cyclopropane intermediates in cracking has been earlier suggested by Sie.[56] However, the path proposed by Sie differs from path HBCP found in our calculations since the former includes cleavage of the C−C bond adjacent to the cyclopropane ring rather than in the ring, and the simultaneous cleavage of two C−C bonds is not required.

Although the three reaction paths found in the calculations are different, they have an important common feature. Indeed, they all include a transition state that represents a complex of the carbocation fragment ($C_4H_9^+$ or $C_5H_{11}^+$) with the negatively charged cluster, whereas both initial and final states represent covalent structures. For instance, the hydrocarbon fragments of the HBCP transition states on the Z_2 cluster bear large positive charges (+0.848 *e* for C_4H_9 and +0.815 *e* for C_5H_{11} according to the NPA scheme at the B3LYP/6-31++G**//B3LYP/6-31G* level) and are not bound to the zeolite cluster with covalent bonds (the shortest C−O distances are 2.382 and 2.302 Å, respectively). In contrast, charges on the hydrocarbon fragments of the corresponding initial states (+0.408 *e* for but-1-oxy and +0.432 *e* for pent-2-oxy) and final state (+0.412 *e* for ethoxy) are much lower, and the fragments are bound to the cluster by covalent bonds C−O (1.469 Å for but-1-oxy, 1.489 Å for pent-2-oxy, and 1.469 Å for ethoxy).

Traditionally, surface carbocations were considered as relatively stable intermediates of the acid-catalyzed transformations,[8−12] similar to the liquid superacid-catalyzed transformations.[15] However over the past years it has been shown that the relatively stable hydrocarbon intermediates are covalent alkoxy species, whereas carbocations represent high-energy activated complexes or transition states.[19−25,57−60] The above-presented results on the β-scission reaction in zeolites indicate that this reaction is similar to others such as olefin chemisorption, protolytic cracking, hydride transfer, and skeletal isomerization having covalent initial and final states and an ionic transition state.

The hydrocarbon fragment $C_4H_9^+$ or $C_5H_{11}^+$ of the transition state, although resembling a carbenium ion, is not free but strongly interacts with the negatively charged cluster. For instance, the energy required for infinite separation of the pent-2-yl cation $C_5H_{11}^+$ and the anionic cluster $(H_3SiO)AlH2(OSiH_3)^-$ from the HBCP transition state of Figure 3 is equal to 71.3 kcal/mol as calculated at the B3LYP/6-31++G**//6-31G* level with the ZPE corrections. Such a strong interaction with the cluster determines the orientation of the hydrocarbon portion with respect to the cluster and strongly influences the reaction path. Indeed, the difference between the three calculated reaction paths RL, HBCP, and HB is in fact connected with the details of interaction between the hydrocarbon portion of the TS and the cluster (see Figures 1−3 and 5). This suggests that in a real zeolite cage the carbocation-like portion interacts with several zeolite oxygen atoms (instead of only two taken into account in the cluster calculations). Consequently, the potential energy surface for the reaction in a real zeolite cage might be even more complex than that found in our present

TABLE 4: Activation Energies (in kcal/mol, Including the ZPE Corrections) for β-Scission of Pent-2-oxy at Different Levels of Geometry Optimization and Single-Point Calculations[a]

	path HBCP (B3LYP/6-31G* optimized)		path HB (HF/6-31G* optimized)	
final energy calculation	cluster Z_1	cluster Z_2	cluster Z_1	cluster Z_2
HF/6-31G*	73.3	62.1	71.6	60.1
HF/6-31++G**	69.0	59.6	66.9	57.5
MP2(FC)/6-31G*	72.1	65.0	73.5	66.5
MP2(FC)/6-31++G**	66.9	62.9	67.8	64.6
B3LYP/6-31G*	64.3	54.5	65.3	55.6
B3LYP/6-31++G**	59.6	52.4	60.0	53.3
ZPE contribution	−3.9	−4.1	−4.2	−4.5

[a] $Z_1 = H(OH)AlH_2(OH)$; $Z_2 = H_3Si(OH)AlH_2(OSiH_3)$.

calculations, and several parallel reaction paths might be kinetically important.

It is difficult to experimentally determine the activation energy for the β-scission reaction since this is a secondary reaction usually accompanied by a number of other processes. However, one can expect that the activation energy for this reaction should be somewhat lower than that for protolytic cracking of alkanes on zeolites. Indeed, the chain route (eq 2) involving the β-scission step is predominant over protolytic cracking (eq 1) provided that the concentration of the adsorbed carbenium ions is sufficient for hydride transfer. Given the available experimental measurements of activation energies for protolytic cracking of alkanes (46−47 kcal/mol for *n*-alkanes from propane to hexane,[14] 40−41 kcal/mol for isobutane[61]), one concludes that all activation energies for β-scission given in Tables 3 and 4, even the lowest one of 52.4 kcal/mol (pent-2-oxy, Z_2 cluster, path HBCP, B3LYP/6-31++G**//B3LYP/6-31G* level), are somewhat overestimated. The same conclusion follows from the comparison of the calculated activation energies with those obtained from the kinetic modeling of the isobutane cracking (20−45 kcal/mol for β-scission of various adsorbed carbenium ions containing 6−9 carbon atoms).[62] The overestimation of the calculated activation energies might have several reasons; the most important of those are the difference in acid strength between the cluster used in calculations and the real zeolite and the dependence of the β-scission activation energy on the number of carbon atoms in hydrocarbon.

Approximate corrections for acid strength and the number of carbon atoms can be made in order to extrapolate the calculated activation energies to the real zeolite and larger hydrocarbons. For this we use the deprotonation energies of the Z_1 and Z_2 clusters (319.2 and 301.9 kcal/mol at the B3LYP/6-31++G**//B3LYP/6-31G* level), the deprotonation energy determined by Brandt et al.[54] for an "average" zeolite (295 kcal/mol), the activation energies calculated at the B3LYP/6-31++G**//B3LYP/6-31G* level for β-scission of pent-2-oxy on Z_1 (59.6 kcal/mol), but-1-oxy on Z_2 (57.4 kcal/mol) and pent-2-oxy on Z_2 (52.4 kcal/mol), and assume a linear dependence of the activation energy ($E^{\#}$) on both the cluster acid strength and the number of methyl groups at the reaction center. The extrapolations lead to the $E^{\#}$ values of about 45 kcal/mol for 4-methylpent-2-oxy and about 40 kcal/mol for 2,4-dimethylpent-2-oxy. The latter value is already realistic since it is close to or lower than those reported for protolytic cracking[14,61] and fits the range found for β-scission in the kinetic modeling.[62]

Of course, the above-proposed corrections to the activation energy are rather rough. Computation of more precise activation energy values will require explicit calculations with large hydrocarbons and large clusters or periodic zeolite structure. This can in principle be achieved using techniques such as combined ab initio and analytical potential functions calculations,[63,64] the integrated MM/MO approach,[65,66] or the plane wave DFT method.[67,68]

5. Conclusion

1. Quantum chemical calculations on the mechanism of the β-scission reaction in zeolites have been performed. It was found that the potential energy surface for this reaction is very complex. Three possible reaction paths were located: path RL, one-step via the "ringlike" TS; path HBCP, two-step via the "hydrogen-bonded" TS and substituted cyclopropane; and path HB, one-step via the "hydrogen-bonded" TS. Path HBCP has the lowest activation barrier.

2. The B3LYP/6-31G* method of geometry optimization predicts that the HBCP path is the main one and is possible for both but-1-oxy and pent-2-oxy β-scission on both $H(OH)AlH_2(OH)$ and $H_3Si(OH)AlH_2(OSiH_3)$ clusters. The RL path is found to be possible for but-1-oxy β-scission on the $H(OH)AlH_2(OH)$ cluster only.

The HF/6-31G* method of geometry optimization predicts the HB path for pent-2-oxy β-scission with both clusters. It was not possible to find a HF/6-31G* path for but-1-oxy β-scission.

3. β-Scission of pent-2-oxy is found to be easier by around 5 kcal/mol than that of but-1-oxy. This shows that an additional methyl group at the reaction center stabilizes the transition state with respect to the initial state.

4. Activation energies ($E^{\#}$) found with the $H_3Si(OH)AlH_2(OSiH_3)$ cluster are around 8 kcal/mol lower than those found with the smaller $H(OH)AlH_2OH$ cluster, due to the lower acid strength of the latter cluster. Final energy calculations at the B3LYP level lead to the $E^{\#}$ values lower by around 7 kcal/mol than those at the HF level, the latter being in turn lower by around 2 kcal/mol than those at the MP2 level. Final energy calculations with the 6-31++G** basis set yield the $E^{\#}$ values which are lower by around 4 kcal/mol than those with the 6-31G* basis set. Geometry optimizations at the B3LYP/6-31G* and HF/6-31G* levels, albeit predicting different reaction paths, lead to close (within 2.1 kcal/mol) values for $E^{\#}$ provided that final energy calculations are performed at the same level.

5. Transition states for all three paths represent a complex of the carbocation fragment ($C_4H_9^+$ or $C_5H_{11}^+$) with the negatively charged cluster, whereas all initial and final states represent covalent structures. The carbocation fragments of the transition states are not free but strongly interact with the negatively charged cluster by Coulomb attraction and hydrogen bonds. Such a strong interaction with the cluster determines the orientation of the hydrocarbon portion with respect to the cluster and strongly influences the reaction path.

Acknowledgment. The financial support of the Dutch Science Foundation program (NWO) is greatly appreciated.

References and Notes

(1) Wojcechowski, B. W.; Corma, A. *Catalytic Cracking: Catalysts, Chemistry and Kinetics*; Dekker: New York, 1986.
(2) Maxwell, I. E.; Stork, W. H. J. In *Introduction to Zeolite Science and Practice*; van Bekkum, H., Flanigen, E. M., Jansen, J. C., Eds.; Elsevier: Amsterdam, 1991; p 571.
(3) Weitkamp, J. *Ind. Eng. Chem. Prod. Res. Dev.* **1982**, *21*, 550.
(4) Weitkamp, J.; Jacobs, P. A.; Martens, J. A. *Appl. Catal.* **1983**, *8*, 123.
(5) Martens, J. A.; Jacobs, P. A.; Weitkamp, J. *Appl. Catal.* **1986**, *20*, 239.
(6) Martens, J. A.; Jacobs, P. A.; Weitkamp, J. *Appl. Catal.* **1986**, *20*, 283.
(7) Buchanan, J. S.; Santiesteban, J. G.; Haag, W. O. *J. Catal.* **1996**, *158*, 279.
(8) Haag, W. O.; Dessau, R. M. In *Proceedings of 8th International Congress on Catalysis*; Dechema: Frankfurt-am-Main, 1984; Vol. 2, p 305.
(9) Lombardo, E. A.; Pierantozzi, R.; Hall, W. K. *J. Catal.* **1988**, *110*, 171.
(10) Stefanidis, C.; Gates, B. C.; Haag, W. O. *J. Mol. Catal.* **1991**, *67*, 363.
(11) Kranilla, H.; Haag, W. O.; Gates, B. C. *J. Catal.* **1992**, *135*, 115.
(12) Engelhardt, J.; Hall, W. K. *J. Catal.* **1992**, *119*, 108.
(13) Ivanov, S. I.; Timoshenko, V. I. *Kinet. Catal.* **1993**, *34*, 447.
(14) Narbeshuber, T. F.; Vinek, H.; Lercher, J. A. *J. Catal.* **1995**, *157*, 388.
(15) Olah, G. A.; Prakash, G. K. S.; Sommer, J. *Superacids*; Wiley-Interscience: New York, 1985.
(16) Sauer, J.; Ugliengo, P.; Garrone, E.; Saunders, V. R. *Chem. Rev.* **1994,** *94*, 2095.
(17) Kramer, G. J.; van Santen, R. A. *Chem. Rev.* **1995**, *95*, 637.
(18) Blaszkowski, S. R.; van Santen, R. A. *Top. Catal.* **1997**, *4*, 145.
(19) Kazansky, V. B.; Senchenya, I. N. *J. Catal.* **1989**, *119*, 108.
(20) Senchenya, I. N.; Kazansky, V. B. *Catal. Lett.* **1991**, *8*, 317.
(21) Kazansky, V. B. *Acc. Chem. Res.* **1991**, *24*, 379.
(22) Viruela-Martin, P.; Zikovich-Wilson, C. M.; Corma, A. *J. Phys. Chem.* **1993**, *97*, 13713.
(23) Kramer, G. J.; van Santen, R. A.; Emeis, C. A.; Nowak, A. K. *Nature* **1993**, *363*, 529.
(24) Rigby, A. M.; Kramer, G. J.; van Santen, R. A. *J. Catal.* **1997**, *170*, 1.
(25) Kramer, G. J.; van Santen, R. A. *J. Am. Chem. Soc.* **1995**, *117*, 1766.
(26) Kazansky, V. B.; Senchenya, I. N.; Frash, M. V.; van Santen, R. A. *Catal. Lett.* **1994**, *27*, 345.
(27) Collins, S. J.; O'Malley, P. J. *J. Catal.* **1995**, *153*, 94.
(28) Collins, S. J.; O'Malley, P. J. *Chem. Phys. Lett.* **1995**, *246*, 555.
(29) Blaszkowski, S. R.; Nascimento, M. A. C.; van Santen, R. A. *J. Phys. Chem.* **1996**, *100*, 3463.
(30) Kazansky, V. B.; Frash, M. V.; van Santen, R. A. *Appl. Catal. A* **1996**, *146*, 225.
(31) Frisch, M. J.; Trucks, G. W.; Schlegel, H. B.; Gill, P. M. W.; Johnson, B. G.; Robb, M. A.; Cheeseman, J. R.; Keith, T.; Petersson, G. A.; Montgomery, J. A.; Raghavachari, K.; Al-Laham, M. A.; Zakrzewski, V. G.; Ortiz, J. V.; Foresman, J. B.; Cioslowski, J.; Stefanov, B. B.; Nanayakkara, A.; Challacombe, M.; Peng, C. Y.; Ayala, P. Y.; Chen, W.; Wong, M. W.; Andres, J. L.; Replogle, E. S.; Gomperts, R.; Martin, R. L.; Fox, D. J.; Binkley, J. S.; Defrees, D. J.; Baker, J.; Stewart, J. P.; Head-Gordon, M.; Gonzalez, C.; Pople, J. A. *Gaussian 94*, Revision B.3; Gaussian, Inc.: Pittsburgh, PA, 1995.
(32) Carpenter, J. E.; Weinhold, F. *J. Mol. Struct. (THEOCHEM.)* **1988,** *169*, 41.
(33) Glendening, E. D.; Reed, A. E.; Carpenter, J. E.; Weinhold, F. NBO, Version 3.1.
(34) Bates, S.; Dwyer, J. *J. Mol. Struct. (THEOCHEM.)* **1994**, *112*, 57.
(35) Haase, F.; Sauer, J. *J. Am. Chem. Soc.* **1995**, *117*, 3780.
(36) Limtrackul, J.; Yoinuan, J.; Tantanak, D. *J. Mol. Struct. (THEOCHEM.)* **1995**, *332*, 151.
(37) Beck, L. W.; Xu, T.; Nicholas, J. B.; Haw, J. F. *J. Am. Chem. Soc.* **1995**, *117*, 11594.
(38) Broclawik, E.; Himei, H.; Yamadaya, M.; Kubo, M.; Miyamoto, A.; Vetrivel, R. *J. Chem. Phys.* **1995**, *103*, 2102.
(39) Himei, H.; Yamadaya, M.; Kubo, M.; Vetrivel, R.; Broclawik, E.; Miyamoto, A. *J. Phys. Chem.* **1995**, *99*, 12461.
(40) Capitan, M. J.; Odriozola, J. A.; Marquez, A.; Fernandez Sanz, J. *J. Catal.* **1995**, *156*, 273.
(41) Ugliengo, P.; Ferrari, A. M.; Zecchina, A.; Garrone, E. *J. Phys. Chem.* **1996**, *100*, 3632.
(42) Krossner, M.; Sauer, J. *J. Phys. Chem.* **1996**, *100*, 6199.
(43) Blaszkowski, S. R.; van Santen, R. A. *J. Am. Chem. Soc.* **1996**, *118*, 5152.
(44) Arbuznikov, A. V.; Zhidomirov, G. M. *Catal. Lett.* **1996**, *40*, 17.
(45) Evleth, E. M.; Kassab, E.; Jessri, H.; Allavena, M.; Montero, L.; Sierra, L. R. *J. Phys. Chem.* **1996,** *100*, 11368.
(46) Mota, C. J. A.; Esteves, P. M.; de Amorin, M. B. *J. Phys. Chem.* **1996**, *100*, 12418.
(47) Sinclair, P. E.; Catlow, C. R. A. *J. Phys. Chem. B* **1997**, *101*, 295.
(48) Sinclair, P. E.; Catlow, C. R. A. *J. Chem. Soc., Faraday Trans.* **1997**, *93*, 333.
(49) Blaszkowski, S. R.; van Santen, R. A. *J. Phys. Chem. B* **1997**, *101*, 2292.
(50) (a) Becke, A. D. *J. Chem. Phys.* **1993,** *98*, 1372. (b) Becke, A. D. *J. Chem. Phys.* **1993,** *98*, 5648.
(51) Lee, C.; Yang, W.; Parr, R. G. *Phys. Rev. B* **1988,** *37*, 785.
(52) Hehre, W. J.; Radom, L.; Schleyer, P. v R.; Pople, J. A. *An Initio Molecular Orbital Theory*; John Wiley and Sons: New York, 1986.
(53) Dunning, T. H., Jr.; Hay, P. J. In *Modern Theoretical Chemistry*; Schaefer, III, H. F., Ed.; Plenum: New York, 1976; pp 1−28.
(54) Brandt, H. V.; Curtiss, L. A.; Iton, L. E. *J. Phys. Chem.* **1993**, *97*, 12773.
(55) Ramachandran, S.; Lenz, T. G.; Skiff, W. M.; Rappe, A. K. *J. Phys. Chem.* **1996**, *100*, 5898.
(56) Sie, T. *Ind. Eng. Chem. Prod. Res. Dev.* **1992**, *31*, 1881.
(57) Kazansky, V. B. *Stud. Surf. Sci. Catal.* **1994**, *85* (Advanced Zeolite Science and Applications); Jansen, J. C., Stoecker, M., Karge, H. G., Weitkamp, J., Eds.; Elsevier: Amsterdam, 1994; p 251.
(58) Aronson, M. T.; Gorte, R. J.; Farneth, W. E.; White, D. *J. Am. Chem. Soc.* **1989**, *111*, 840.
(59) Haw, J. F.; Richardson, B. R.; Oshiro, I. S.; Lado, N. D.; Speed, J. A. *J. Am. Chem. Soc.* **1989**, *111*, 2052.
(60) Haw, J. F.; Nicholas, J. B.; Xu, T.; Beck, L. W.; Ferguson, D. B. *Acc. Chem. Res.* **1996**, *29*, 259.
(61) Corma, A.; Miguel, P. J.; Orchilles, A. V. *J. Catal.* **1994**, *145*, 171.
(62) Yaluris, G.; Rekoske, J. E.; Aparicio, L. M.; Madon, R. J.; Dumesic, J. A. *J. Catal.* **1995**, *153*, 54.
(63) Eichler, U.; Kölmel, C. M.; Sauer, J. *J. Comput. Chem.* **1996**, *18*, 463.
(64) Brandle, M.; Sauer, J. *J. Mol. Catal. A* **1997**, *119*, 19.
(65) Matsubara, T.; Maseras, F.; Koga, N.; Morokuma, K. *J. Phys. Chem.* **1996**, *100*, 2573.
(66) Froese, R. D. J.; Humbel, S.; Svensson, M.; Morokuma, K. *J. Phys. Chem. A* **1997**, *101*, 227.
(67) Shah, R.; Gale, J. D.; Payne, M. C. *J. Phys. Chem.* **1996**, *100*, 11688.
(68) Shah, R.; Gale, J. D.; Payne, M. C. *J. Phys. Chem. B* **1997**, *101*, 4787.